PHYSICAL REVIEW D

PARTICLES AND FIELDS

THIRD SERIES, VOLUME 42, NUMBER 3 1 AUGUST 1990

Charged-particle multiplicities in e^+e^- annihilations at $\sqrt{s}$ = 50–61.4 GeV

H. W. Zheng,[a] P. Perez,[a] P. Auchincloss,[a] D. Blanis,[a] A. Bodek,[a] H. Budd,[a] S. Eno,[a] C. A. Fry,[a,h] H. Harada,[a] Y. H. Ho,[a] Y. K. Kim,[a] T. Kumita,[a] T. Mori,[a] S. L. Olsen,[a,i] N. M. Shaw,[a] A. Sill,[a] E. H. Thorndike,[a] K. Ueno,[a] R. Imlay,[b] P. Kirk,[b] J. Lim,[b] R. R. McNeil,[b] W. Metcalf,[b] S. S. Myung,[b] C. P. Cheng,[c] P. Gu,[c] J. Li,[c] Y. K. Li,[c,e] M. H. Ye,[c] Y. C. Zhu,[c] A. Abashian,[d] K. Gotow,[d] K. P. Hu,[d] E. H. Low,[d] M. E. Mattson,[d] L. Piilonen,[d] K. L. Sterner,[d] S. Lusin,[e] C. Rosenfeld,[e] A. T. M. Wang,[e] S. Wilson,[e] M. Frautschi,[f] H. Kagan,[f] R. Kass,[f] C. G. Trahern,[f] R. E. Breedon,[g,h] G. N. Kim,[g,h] Winston Ko,[g] R. L. Lander,[g] K. Maeshima,[g] R. L. Malchow,[g] J. R. Smith,[g] D. Stuart,[g] K. Abe,[h] Y. Fujii,[h] Y. Higashi,[h] S. K. Kim,[h] Y. Kurihara,[h] A. Maki,[h] T. Nozaki,[h] T. Omori,[h] H. Sagawa,[h] Y. Sakai,[h] Y. Sugimoto,[h] Y. Takaiwa,[h] S. Terada,[h] R. Walker,[h,a] F. Kajino,[j] D. Perticone,[k] R. Poling,[k] T. Thomas,[k] Y. Ishi,[l] K. Miyano,[l] H. Miyata,[l] T. Sasaki,[l] Y. Yamashita,[m] A. Bacala,[n,o] J. Liu,[n] I. H. Park,[n] F. Sannes,[n] S. Schnetzer,[n] R. Stone,[n] J. Vinson,[n] S. Kobayashi,[p] A. Murakami,[p] J. S. Kang,[q] H. J. Kim,[q] M. H. Lee,[q] D. H. Han,[r] E. J. Kim,[r] D. Son,[r] T. Kojima,[s] S. Matsumoto,[s] R. Tanaka,[s] Y. Yamagishi,[s] T. Yasuda,[s] T. Ishizuka,[u] and K. Ohta[u]

(The AMY Collaboration)

[a]*University of Rochester, Rochester, New York 14627*
[b]*Louisiana State University, Baton Rouge, Louisiana 70803*
[c]*Institute of High Energy Physics, Beijing 100039*
[d]*Virginia Polytechnic Institute and State University, Blacksburg, Virginia 24061*
[e]*University of South Carolina, Columbia, South Carolina 29208*
[f]*Ohio State University, Columbus, Ohio 43210*
[g]*University of California, Davis, California 95616*
[h]*KEK, National Laboratory for High Energy Physics, Ibaraki 305*
[i]*Tsukuba University, Ibaraki 305*
[j]*Konan University, Kobe 658*
[k]*University of Minnesota, Minneapolis, Minnesota 55455*
[l]*Niigata University, Niigata 950-21*
[m]*Nihon Dental College, Niigata 951*
[n]*Rutgers University, Piscataway, New Jersey 08854*
[o]*University of the Philippines, Quezon City, 3004*
[p]*Saga University, Saga 840*
[q]*Korea University, Seoul 136-701*
[r]*Kyungpook National University, Taegu 702-701*
[s]*Chuo University, Tokyo 112*
[u]*Saitama University, Urawa 338*
(Received 5 March 1990)

We present the charged-particle multiplicity distributions for e^+e^- annihilation at center-of-mass energies from 50 to 61.4 GeV. The results are based on a data sample corresponding to a total integrated luminosity of 30 pb^{-1} obtained with the AMY detector at the KEK storage ring TRISTAN. The charged-particle multiplicity distributions deviate significantly from the modified Poisson and pair Poisson distributions, but follow Koba-Nielsen-Olesen scaling and are well reproduced by the LUND parton-shower model.

I. INTRODUCTION

The reaction $e^+e^- \to (\gamma, Z) \to$ hadrons is quite simple at the parton level and thus provides for relatively unambiguous studies of the fragmentation of partons. The charged-particle multiplicity in this reaction is one of the most basic observables in the fragmentation process. It has been measured whenever a new energy regime has been accessed.

In the absence of a fundamental theory, a number of phenomenological models, starting with Heisenberg in 1939,[1] have been proposed to characterize the charged multiplicity in high-energy hadron processes. In 1950, Fermi used statistical arguments to predict that the average number of charged particles produced in high-energy collisions would increase with increasing center-of-mass energy ($\sqrt{s}$) as[2]

$$\langle n \rangle = a s^{1/4} .$$

More recent models, motivated by perturbative QCD calculations of the evolution of partons in a leading-logarithm approximation, predict

$$\langle n \rangle = a + b \exp\{[c \ln(s/Q_0^2)]^{1/2}\} ,$$

where Q_0 is related to the Λ cutoff parameter of QCD.[3-5] An analysis of pp data suggests the empirical form[6]

$$\langle n \rangle = a + b \ln s + c \ln^2 s .$$

There has also been considerable interest in the shape of the distributions of multiplicities at a given energy. In 1972, Koba, Nielsen, and Olesen[7] (KNO), starting from Feynman scaling[8] and with no further dynamical assumptions, derived the asymptotic result that the product of the mean charged multiplicity $\langle n \rangle$ and the probability $P(n)$ for n charged particles in the final state is given by a universal function:

$$\psi\left[\frac{n}{\langle n \rangle}\right] = P(n)\langle n \rangle .$$

If the charged multiplicity distribution obeys KNO scaling, then the dispersion $D = (\langle n^2 \rangle - \langle n \rangle^2)^{1/2}$ is proportional to $\langle n \rangle$.

Chou and Yang[9] used a different approach and argued that the production of so many particles is indicative of a stochastic process and, thus, should have a Poisson-type behavior. In this case $D \propto \sqrt{\langle n \rangle}$, which means that at sufficiently high energies the distribution would be narrower than that expected from KNO scaling.

The comparison of the charged-particle multiplicity distribution with Poisson expectations is complicated by the fact that, since electric charge is conserved, charged particles are always produced in pairs. The HRS experiment reported charged multiplicity distributions at $\sqrt{s} = 29$ GeV which are in excellent agreement with the "modified Poisson" form[10]

$$P^{\text{mod}}(n) = \begin{cases} 2\dfrac{\langle n \rangle^n e^{-\langle n \rangle}}{n!}, & n = \text{even} , \\ 0, & n = \text{odd} . \end{cases}$$

A modified Poisson has a rms width $D = \sqrt{\langle n \rangle}$. The TASSO experiment has also reported data at $\sqrt{s} = 14$, 22 GeV that followed a modified Poisson behavior. At $\sqrt{s} = 34.8$ and 43.6 GeV, however, they observed significant deviations from this form.[11] In fact, if one attributes a Poisson-type behavior to the pairwise production of charged particles, one expects a "pair Poisson" distribution of the form

$$P^{\text{pair}}(n) = \begin{cases} \dfrac{(\langle n \rangle/2)^{n/2} e^{-\langle n \rangle/2}}{(n/2)!}, & n = \text{even} , \\ 0, & n = \text{odd} . \end{cases}$$

This pair Poisson distribution has $D = \sqrt{2\langle n \rangle}$, which is considerably broader than the measured values.

While the KNO scaling function is usually taken to be a "Γ distribution,"

$$\psi(Z) = \frac{K^K}{\Gamma(K)} Z^{K-1} e^{-KZ} , \tag{1}$$

where $Z = n/\langle n \rangle$ is the scaled multiplicity, it has been observed that multiplicity distributions in high-energy hadronic, leptonic, and semileptonic processes can be quite well described by negative-binomial distributions.[12-15] These distributions can be represented in the form

$$P(n, \langle n \rangle, k) = \frac{k(k+1)\cdots(k+n-1)}{n!} \times \left[\frac{\langle n \rangle}{\langle n \rangle + k}\right]^n \left[\frac{k}{\langle n \rangle + k}\right]^k , \tag{2}$$

where k is related to the dispersion D by

$$\frac{D^2}{\langle n \rangle^2} = \frac{1}{\langle n \rangle} + \frac{1}{k} .$$

This function gives KNO scaling [Eq. (1)] in the limit of $\langle n \rangle$ much larger than k. [Equation (2) is an ordinary binomial distribution when k is a negative integer; in the limit of $k \to \infty$, it has a Poisson form.] Negative-binomial distributions are characteristic of cascade-type (or shower) mechanisms for multiparticle production.[12]

In this paper we report a measurement of the charged-particle multiplicity for e^+e^- annihilations into multihadron final states which has been obtained with the AMY detector at the KEK storage ring TRISTAN. Our data sample consists of more than 3000 events at center-of-mass energies between 50 and 61.4 GeV. We compare our results with those of previous experiments and with predictions of various models, including the LUND 6.3 parton-shower model.[16] The paper is arranged as follows. In Sec. II, we briefly describe the AMY detector. Event- and track-selection criteria are discussed in Sec. III. Sections IV and V provide descriptions of the detector simulation and data correction procedure. Section VI presents a study of the systematic uncertainties in our measurements. In Sec. VII, we present the fully corrected charged multiplicity results, and discuss the energy dependence of the average charged multiplicity, the shape of multiplicity distribution, and KNO scaling. We give a brief discussion of the results in Sec. VIII.

II. THE AMY DETECTOR

The AMY detector, including its trigger and luminosity determination procedures, has been described elsewhere.[17] Here we mention only those features that are essential for the measurement of the charged multiplicity. The central feature of the detector is a 3-T superconducting solenoid magnet enclosing tracking and electromagnetic shower detectors. Charged-particle tracking is provided by a four-layer cylindrical array of drift tubes (ITC), followed by a cylindrical drift chamber (CDC). The CDC extends from an inner radius of 15 cm to an outer radius of 65 cm. Its 25 axial and 15 stereo (typical angle $\sim 5°$) layers contain 9048 active cells. Charged particles are detected efficiently over the polar-angle region $|\cos\theta| < 0.87$, with a momentum resolution $\Delta p_t/p_t \simeq 0.6\%[p_t \text{ (GeV}/c)]$. Outside the CDC is a cylindrical electromagnetic calorimeter (SHC) with a total thickness of 15 radiation lengths. The SHC covers the angular region $|\cos\theta| < 0.73$. In addition to these components, there are muon detectors surrounding the magnet iron return yoke, and end-cap calorimeters that are not used in the present analysis.

The reliability of our multiplicity determination is enhanced by the relatively small amount of material encountered by charged particles and photons as they emerge from the interaction region. The vacuum pipe of TRISTAN is aluminum with a wall thickness of 1.5 mm. The ITC is constructed of polystyrene and epoxy, and the inner cylinder of the CDC vessel is made of carbon-fiber reinforced plastic. Radially, the material between the interaction point and the first tracking layer of the CDC corresponds to 3.0% of a radiation length and 0.7% of an interaction length. This relatively thin front end, combined with the high magnetic field, minimizes the number of spurious charged tracks resulting from photon conversions and nuclear interactions.

Multihadron e^+e^- annihilation events were triggered by large energy pulses in the SHC or by the presence of many track segments in the tracking system. By comparing redundant triggers, we have determined that the overall trigger efficiency for the selected multihadron annihilation events is greater than 99.7%.[18]

III. EVENT SELECTION

The crucial component of our measurement of charged multiplicity is the reliable reconstruction of charged tracks in the CDC. Track candidates were required to have at least eight axial and five stereo hits which could be well fitted to a helix. Each track was required to originate in a cylindrical fiducial volume, centered on the interaction point, with a 5-cm radius in the plane (r,ϕ) transverse to the beam direction, and a length of 30 cm along the beam direction (z). A polar angle cut of $|\cos\theta| < 0.85$ ensured that high-momentum tracks traversed all forty CDC layers. The small number of hits required, in comparison to the total number possible, helps keep the track-reconstruction efficiency high, particularly for particles with low momentum and those that are inside tightly collimated jets. The momentum of each charged track was required to be greater than 0.2 GeV/c. Charged particles originating from K_S^0, Λ^0, and heavy-meson and baryon decays are included as primary charged particles.

Another component of our event-selection procedure was the amount of energy deposited in the electromagnetic calorimeter by photons. Clusters in the SHC were declared photons if their energy was at least 1 GeV, or if their energy was between 0.2 and 1.0 GeV and there were no charged tracks within 3 cm.

Criteria for the selection of multihadron events were chosen based on a Monte Carlo study of the response of the AMY detector to simulated e^+e^- annihilations into hadronic final states. The input parameters of the simulation were adjusted to reproduce the experimentally observed distributions of the variables used in the selection process.

To be accepted for our analysis, an event was required to have at least five well reconstructed charged tracks, a total visible energy greater than one-half of the center-of-mass energy, a momentum imbalance along the beam direction of no more than 40% of the visible energy, and more than 3 (5) GeV energy in the SHC for the data collected at center-of-mass energies of 50 and 52 (55–61.4) GeV.

From the z-vertex distribution obtained with the cut on z relaxed, we deduced that the contamination from beam-gas collisions was less than 0.3%. Monte Carlo simulations indicated that contaminations from $e^+e^- \to \tau^+\tau^-$ and two-photon processes ($e^+e^- \to e^+e^-$ + hadrons) were 0.6–0.9 % and 0.6–0.7 %, respectively, depending on the beam energy.[18] In order to restrict our multiplicity analysis to those events for which the track acceptance is high, we further required that the polar angle (θ_T) of the thrust axis of each event, determined from the charged particles alone, be such that $|\cos\theta_T| < 0.70$.

IV. DETECTOR SIMULATION AND PERFORMANCE

The charged-particle reconstruction efficiency of the spectrometer was determined by means of a detailed Monte Carlo simulation of the detector. This simulation was also used to correct the observed distributions for acceptance and resolution smearing.

The generation of e^+e^- annihilation events was done with the LUND 6.3 parton-shower program using default values of the input parameters[19] and including the effects of QED initial-state radiation. The generated particles were propagated through the detector and their interactions, as well as the response of the drift chamber and calorimeter, simulated. Data records similar to those from real events were created and subjected to the same selection and reconstruction procedures as were used for real events.

The overall detection efficiency for multihadron events passing the cut on the thrust angle was determined from the Monte Carlo studies to be (55±2) %. The track-reconstruction efficiency for isolated tracks with $|\cos\theta| < 0.85$ and transverse momentum above 0.4 GeV/c was also determined from the simulation and found to be

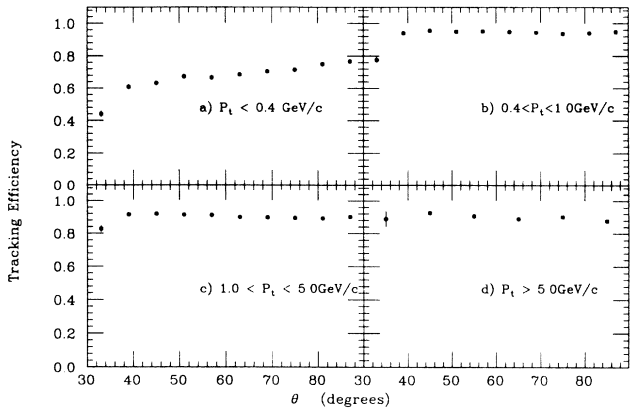

FIG. 1. The track-reconstruction efficiency as a function of θ, the polar angle with respect to the e^+e^- beam direction. Four different transverse-momentum intervals are shown: (a) $p_t < 0.4$ GeV/c; (b) $0.4 < p_t < 1.0$ GeV/c; (c) $1.0 < p_t < 5.0$ GeV/c; (d) $p_t > 5.0$ GeV/c.

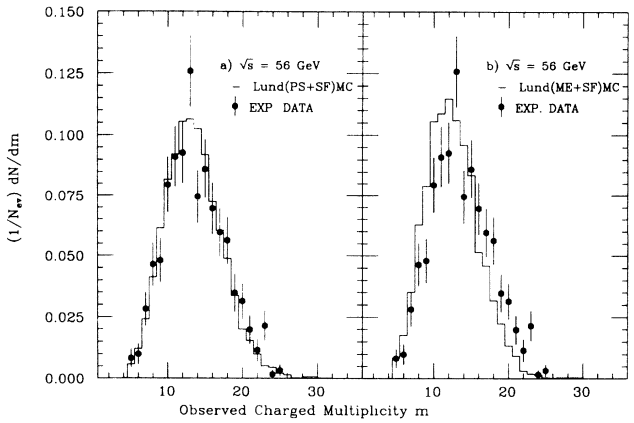

FIG. 2. The observed charged multiplicity distribution at $\sqrt{s} = 56$ GeV compared with simulated events generated with (a) the LUND 6.3 (parton-shower) and (b) the LUND 6.2 (matrix-element) Monte Carlo event generators.

99%. Sometimes, however, tracks in tightly collimated jets can be missed. From Monte Carlo studies we found that for charged particles with $p_t > 0.4$ GeV/c and $|\cos\theta| \leq 0.85$ the average efficiency is 95%. A detailed examination, using the Monte Carlo studies, showed that the missed tracks are almost always lost because of confusion with other nearby tracks.[20] The tracking efficiency in hadronic events is displayed as a function of the transverse momentum and the polar angle of the tracks in Fig. 1. There is a cutoff for transverse momenta lower than 0.2 GeV/c, in which case the particles barely enter the CDC; particles with $p_t \geq 0.4$ GeV/c traverse the entire radial extent of the chamber. For all transverse momenta the efficiency depends weakly on the polar angle of the track for values of $\theta > 36°$.

V. OBSERVED MULTIPLICITY DISTRIBUTION AND CORRECTIONS

The observed multiplicity distribution for the 56-GeV data sample is shown in Fig. 2(a). The corresponding distribution for the simulated event sample is plotted as a histogram. The agreement is quite good. In order to extract the true multiplicity distribution, it is necessary to correct for the loss of charged particles due to incomplete acceptance and imperfect track finding. In addition, initial-state radiation decreases the center-of-mass energy of the annihilating e^+e^- pair, and further reduces the observed charged multiplicity. On the other hand, the conversion of γ rays to e^+e^- pairs and the nuclear interactions of hadrons in the material of the inner part of the detector can generate extra charged particles. The data were corrected for all of these effects.

The correction procedure was based on Monte Carlo–simulated events generated using the LUND 6.3 parton-shower model. The first step was to correct for detector effects. We defined the true multiplicity of an event as the total number of charged particles generated by the Monte Carlo simulation, including the effects of QED initial-state radiation, at any angle and momentum. As is customary for these measurements, we let all of the strange hyperons, K_S^0, charm, and beauty particles decay at the generator level, and, thus, charged particles among their decay products are included in the true multiplicity.[21] The frequency for events generated with n tracks to be observed with m tracks was obtained after applying the analysis cuts to reconstructed simulated events. This was used to determine a correction matrix for use in obtaining the true multiplicity distribution from the observed distribution.

The element $A(n,m)$ of the correction matrix is defined to be the fraction of those events with m observed tracks that have a true multiplicity n:

$$A(n,m) = \frac{\text{No. of events with } n \text{ tracks generated and } m \text{ tracks observed}}{\text{No. of events with } m \text{ tracks observed}} .$$

In $A(n,m)$, we included an extra column, $m = m_{\text{fail}}$, where we tallied the normalized multiplicity distribution of the generated events that failed the acceptance and selection cuts. For fixed (true multiplicity) n, $A(n,m)$ is the distribution of the observed values of m, as illustrated in Fig. 3. The root-mean-squared spread of the observed number of tracks versus the true number of particles is indicated by the closed curve in Fig. 4. On average, there is a loss of charged particles, but, as can be seen in Figs. 3 and 4, the observed multiplicity is sometimes larger than the true multiplicity. At low multiplicities, the average observed number of tracks is only slightly smaller than the generated number. For high-multiplicity events, however, the distortion is substantial. The true multipli-

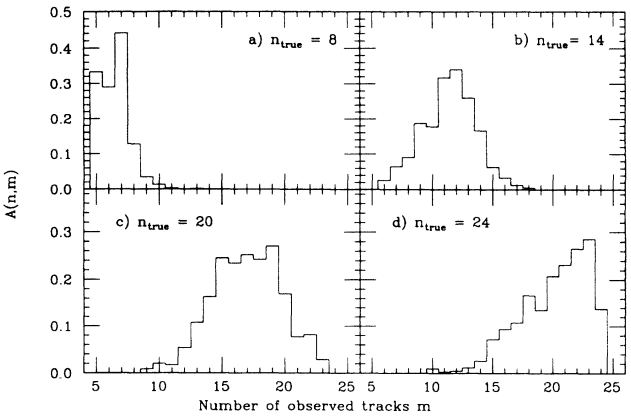

FIG. 3. The observed multiplicity distributions $[A(m,n)]$ for generated multiplicities of $n=8$ (a), 14 (b), 20 (c), and 24(d), as determined from the 56-GeV Monte Carlo–simulated data sample.

city distribution $N_{\text{gen}}^{\text{MC}}$ generated by Monte Carlo simulation and the observed multiplicity distribution $N_{\text{obs}}^{\text{MC}}$ are related by

$$N_{\text{gen}}^{\text{MC}}(n)=\sum_m A(n,m)N_{\text{obs}}^{\text{MC}}(m) .$$

The entry $N_{\text{obs}}^{\text{MC}}(m_{\text{fail}})$ is the number of generated events that fail to survive the acceptance and selection criteria.

The second step was to correct for the effects of QCD initial-state radiation. We define a correction factor as

$$C(n)=\frac{\rho(n)_{\text{gen}}^{\text{NR}}}{\rho(n)_{\text{gen}}^{\text{RD}}} ,$$

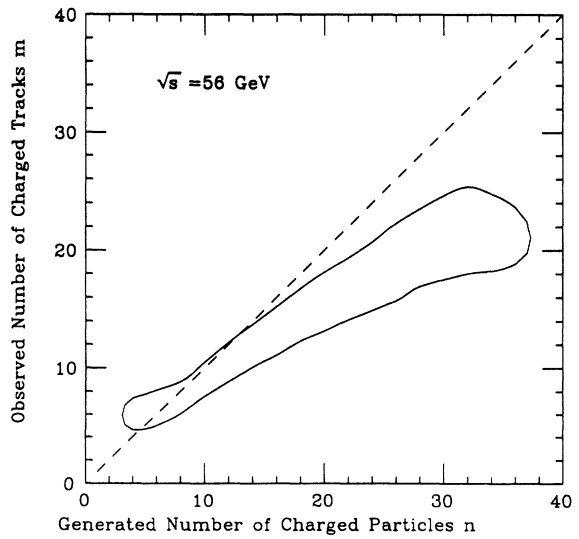

FIG. 4. The enclosed area indicates the rms range in values of the observed charged multiplicity m for different values of the generated multiplicity n, as determined from simulated Monte Carlo events. The dashed line corresponds to $m=n$.

where $\rho(n)_{\text{gen}}^{\text{RD}}$ and $\rho(n)_{\text{gen}}^{\text{NR}}$ are the normalized multiplicity distributions for events generated with the QED initial-state radiation turned on and off, respectively. For n values that occur with significant probability, the correction factors are near 1. For example, for n equal to 10, the factor is 0.7, and for n equal to 30, it is 1.4.

We obtained the corrected charged-particle multiplicity distribution $N_{\text{cor}}(n)$ from

$$N_{\text{cor}}(n)=C(n)\sum_m A(n,m)N_{\text{obs}}(m) ,$$

where $N_{\text{obs}}(m)$ is the observed charged-particle multiplicity distribution of final selected experimental data. The entry $N_{\text{obs}}(m_{\text{fail}})$ was determined from the estimated acceptance and selection efficiency.

Because of the event-selection requirement of five or more observed charged tracks, the lowest value of n where $N_{\text{cor}}(n)$ is directly derived from the data was $n=6$. The values of $N_{\text{cor}}(n)$ for $n=2$ and 4 were deduced from the Monte Carlo prediction after normalizing to the data.

VI. SYSTEMATIC ERRORS

We studied seven possible sources of systematic uncertainty in our multiplicity determination. The procedures used to estimate the systematic errors are described below. Table I summarizes the results.

(1) Since the events that fail our acceptance and selection criteria have a different multiplicity distribution than those that pass, our results depend upon our understanding of the efficiency of these cuts, which is determined from the simulated event sample. By examining how the estimated acceptance changes when different Monte Carlo event generators and different versions of the detector simulation algorithms are used, we determined a 2% uncertainty for this efficiency. A more detailed description of the acceptance calculation and the estimates of its uncertainty is given in Ref. 18. Varying the efficiency by this amount results in a 0.3% change in the resulting value of $\langle n \rangle$, which we have taken as the systematic error caused by this effect.

(2) We relied on the detector simulation to determine the track-finding efficiency. To test our sensitivity to the details of the simulation, we changed the CDC smearing parameters over a somewhat exaggerated range and ex-

TABLE I. Summary of the systematic errors of $\langle n \rangle$.

Systematic errors	(%)
Detection efficiency	0.3
Track-finding efficiency	1.0
Initial-state radiations	0.4
$\gamma \rightarrow e^+e^-$ conversion	0.1
Monte Carlo scheme	2.5
Low multiplicity	0.6
Event selection	0.3
Overall systematic error	2.8

amined the change in the measured charged multiplicity. We found the variation $\Delta\langle n\rangle/\langle n\rangle$ to be less than 1.0% and have used 1% as the systematic error associated with detector smearing.

(3) QED initial-state radiation reduces the center-of-mass energy of the e^+e^- collision, distorting the multiplicity distribution. We corrected for this by using Monte Carlo events with and without initial-state radiation. The average multiplicity $\langle n\rangle$ increased 8% and the dispersion D decreased 7% after the radiation correction. We have determined that the radiative corrections themselves are done with a precision of approximately 5%.[18] We therefore assign a 0.4% systematic error to the correction of $\langle n\rangle$.

(4) The average number of tracks that originate from photon conversions was estimated by the Monte Carlo simulations to be 0.29 per event, or $\sim$2% of the observed multiplicity. We checked the reliability of the Monte Carlo calculation in two ways. The number of photons with energy greater than 2.5 GeV observed in the SHC was compared with the Monte Carlo predictions and yielding agreement at the 99% level. Additionally, photons converting in the beam pipe or ITC were reconstructed in the CDC; their measured number agrees with the Monte Carlo calculation at the 97% level. We estimate that the uncertainty in our measurement due to this correction is 0.1%. Nuclear interactions in the beam pipe and inner material of the detector were modeled using the Monte Carlo program by Grant.[22] Since the interaction probability is one-third that for photon conversion, the systematic error associated with nuclear interactions is expected to be negligibly small.

(5) The correction procedure relies on the QCD event generator. We use the LUND 6.3 (parton-shower) event generator because it has been shown to give an accurate description of the general properties of multihadron events in our energy range.[23] To assess the sensitivity of our results to the details of the event generator, we repeated our analysis with the LUND 6.3 (matrix-element with string-fragmentation) generator.[24] Because this model so inadequately describes the observed charged multiplicity, as can be seen in Fig. 2(b), we have chosen to use one-half of the difference in the results obtained with the two models as our estimate of the systematic error associated with the choice of event generator.[25] This uncertainty corresponds to a 2.5% systematic error for $\langle n\rangle$ and is the dominant systematic error on the individual points of the multiplicity distributions.

(6) Since our event-selection criteria eliminated low-multiplicity events, we must take these results from an extrapolation of the parton-shower-model results. As an estimate of the error associated with these points, we take the difference between the modified Poisson distribution values, which follow the parton-shower-model results in this region fairly closely, and the pair Poisson distribution values, which are higher than the Monte Carlo data, as representative of the range of uncertainty. This gives an estimate of the uncertainty due to the extrapolation to $n=2$ and $N=4$ of 0.6%.

(7) The multihadron event and track-selection criteria could be another source of systematic error. To estimate the magnitude of this uncertainty we changed the selection criteria and examined the effect on the measured charge multiplicity. For example, repeating the entire analysis with the cut on the angle of the thrust axis changed from $|\cos\theta_T|<0.70$, to $|\cos\theta_T|<0.50$, results in a 0.23% change in the average multiplicity. Similar studies of the effects due to the track- and event-selection criteria showed a negligible effect on the measured average multiplicity. We assign a 0.3% systematic error to the effect of the track and event selection.

As is reflected in Table I, we have combined the uncertainties from the sources described in quadrature to obtain an estimate of the overall systematic uncertainty of our multiplicity measurement of 2.8%. A more detailed discussion of the estimation of systematic errors is given in Ref. 20.

VII. CHARGED MULTIPLICITY

The fully corrected multiplicity distributions for the eight center-of-mass energies in our full data sample are listed in Table II; the results for all energies combined ($\langle\sqrt{s}\rangle=57$ GeV) are given in the final column of the table. For each entry, the error stated first indicates the statistical uncertainty and the second gives the estimated systematic error. The $n=2$ and $n=4$ points were derived using the LUND 6.3 Monte Carlo program normalized to the observations for higher n values; the corresponding errors are systematic only. The multiplicity distribution for all energies combined ($\langle\sqrt{s}\rangle=57$ GeV) is shown in Fig. 5. The error bars shown are the quadrature sum of the statistical and systematic errors. There is excellent agreement with the LUND parton-shower model. Neither the modified Poisson nor the pair Poisson distributions

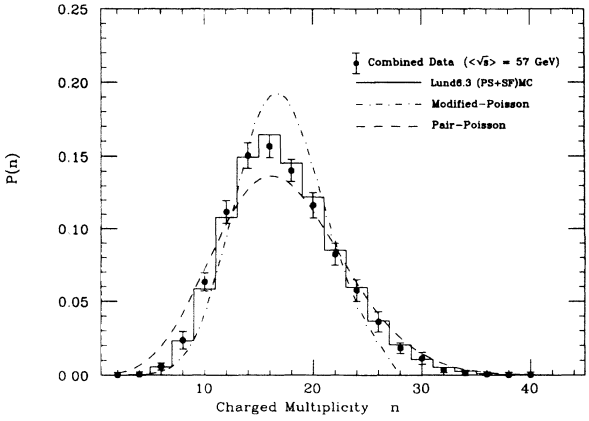

FIG. 5. The corrected charged multiplicity distribution for all energies combined compared with the predictions of the LUND 6.3 (parton-shower and string-fragmentation) model (solid histogram), the modified Poisson (dotted-dash curve), and pair Poisson (dashed curve) distributions. The mean center-of-mass energy is 57 GeV. The errors shown are the quadrature sum of the statistical and systematic errors.

TABLE II. The charged multiplicity distributions $(1/N_{ev})dN/dn$ in percent. The final column lists the results from all energies combined ($\langle\sqrt{s}\rangle = 57$ GeV). Statistical errors are listed first and systematic errors second. For the $n=2$ and $n=4$ points only systematic errors are given.

n	$\sqrt{s}=50$ GeV	$\sqrt{s}=52$ GeV	$\sqrt{s}=55$ GeV
2	0.0127±0.0097	0.0125±0.0094	0.0036±0.0038
4	0.076±0.039	0.074±0.037	0.076±0.035
6	0.68±0.17±0.27	0.638±0.096±0.256	0.72±0.13±0.29
8	3.35±0.97±0.82	3.00±0.42±0.73	2.68±0.48±0.65
10	7.67±2.27±0.64	7.39±0.99±0.62	6.91±1.15±0.58
12	13.90±3.94±0.70	12.96±1.69±0.65	12.40±1.84±0.62
14	18.13±4.98±0.54	16.12±2.07±0.48	16.38±2.37±0.49
16	16.92±4.73±0.12	15.56±2.02±0.11	15.80±2.35±0.12
18	13.95±4.25±0.18	14.15±1.96±0.18	14.04±2.22±0.18
20	9.98±3.58±0.50	11.24±1.80±0.56	12.03±2.11±0.60
22	6.05±2.41±0.39	7.14±1.31±0.46	7.92±1.58±0.52
24	4.34±1.96±0.45	5.37±1.19±0.56	5.03±1.08±0.52
26	2.41±1.20±0.40	3.03±0.85±0.50	3.06±0.80±0.50
28	1.37±0.66±0.22	1.69±0.47±0.28	1.41±0.39±0.23
30	0.84±0.43±0.28	1.19±0.46±0.39	0.86±0.30±0.28
32	0.18±0.12±0.08	0.27±0.11±0.12	0.29±0.14±0.13
34	0.09±0.05±0.01	0.11±0.06±0.02	0.33±0.27±0.05
36	0.04±0.03±0.07	0.04±0.02±0.06	0.04±0.03±0.07
38	0.02±0.02±0.03	0.03±0.02±0.06	0.02±0.02±0.04

n	$\sqrt{s}=56$ GeV	$\sqrt{s}=57$ GeV	$\sqrt{s}=60$ GeV
2	0.0058±0.0061	0.0025±0.0026	0.0082±0.0085
4	0.069±0.033	0.065±0.031	0.071±0.036
6	0.66±0.08±0.26	0.72±0.11±0.29	0.49±0.09±0.20
8	2.61±0.28±0.64	2.58±0.37±0.63	2.00±0.34±0.49
10	6.67±0.74±0.56	6.11±0.81±0.51	5.77±0.88±0.48
12	11.04±1.18±0.55	10.15±1.36±0.51	11.01±1.59±0.55
14	15.17±1.52±0.45	14.33±1.81±0.42	13.24±1.89±0.39
16	15.54±1.58±0.11	15.04±1.93±0.11	15.27±2.21±0.11
18	14.08±1.58±0.18	14.82±1.96±0.19	13.89±2.11±0.17
20	11.66±1.46±0.58	12.75±1.88±0.64	11.33±1.89±0.57
22	8.55±1.20±0.56	9.09±1.54±0.59	10.00±1.87±0.65
24	5.71±0.93±0.59	5.95±1.21±0.62	6.48±1.40±0.67
26	3.76±0.76±0.62	4.09±1.00±0.68	4.91±1.22±0.81
28	2.06±0.46±0.34	1.88±0.53±0.31	2.53±0.84±0.41
30	1.38±0.35±0.45	1.33±0.51±0.43	1.20±0.41±0.39
32	0.76±0.22±0.34	0.72±0.27±0.33	0.93±0.48±0.42
34	0.14±0.06±0.02	0.25±0.13±0.04	0.46±0.23±0.07
36	0.10±0.04±0.19	0.05±0.03±0.10	0.26±0.24±0.48
38	0.01±0.01±0.02	0.08±0.04±0.14	0.13±0.10±0.23
40			0.01±0.01±0.02

n	$\sqrt{s}=60.8$ GeV	$\sqrt{s}=61.4$ GeV	$\langle\sqrt{s}\rangle=57$ GeV (combined data)
2	0.0024±0.0025	0.0023±0.0025	0.0032±0.0014
4	0.041±0.018	0.040±0.018	0.050±0.020
6	0.51±0.09±0.21	0.49±0.08±0.20	0.59±0.03±0.24
8	2.06±0.34±0.50	1.94±0.29±0.47	2.35±0.13±0.58
10	5.76±0.93±0.48	5.84±0.85±0.49	6.33±0.33±0.53
12	10.36±1.59±0.52	10.98±1.51±0.55	11.19±0.56±0.56
14	14.77±2.11±0.44	15.42±1.99±0.46	15.03±0.72±0.45
16	16.30±2.38±0.12	16.29±2.17±0.12	15.66±0.76±0.11
18	13.88±2.14±0.17	13.39±1.91±0.17	14.04±0.73±0.18
20	11.81±1.90±0.59	11.30±1.69±0.57	11.64±0.66±0.58
22	8.50±1.64±0.55	8.11±1.45±0.53	8.23±0.54±0.54
24	6.68±1.47±0.69	6.42±1.33±0.66	5.75±0.44±0.60

TABLE II. (*Continued*).

n	$\sqrt{s}=60.8$ GeV	$\sqrt{s}=61.4$ GeV	$\langle\sqrt{s}\rangle=57$ GeV (combined data)
26	4.21±1.17±0.70	4.26±1.09±0.71	3.61±0.34±0.60
28	2.37±0.70±0.39	2.53±0.73±0.41	1.84±0.19±0.30
30	1.24±0.41±0.40	1.43±0.47±0.47	1.15±0.14±0.38
32	0.76±0.28±0.35	0.81±0.28±0.37	0.37±0.06±0.17
34	0.46±0.20±0.07	0.42±0.16±0.06	0.14±0.03±0.02
36	0.24±0.14±0.44	0.20±0.10±0.36	0.05±0.01±0.09
38	0.01±0.01±0.01	0.02±0.01±0.03	0.01±0.01±0.09
40	0.05±0.02±0.09	0.10±0.05±0.18	0.01±0.01±0.09

provide good representations of the data. Summaries of the characteristics of the eight data sets and of the properties of the multiplicity distributions are listed in Table III. Of particular note are the f_2 moments, where $f_2=D^2-\langle n\rangle$. These are statistically significantly nonzero, reflecting the large disagreement between the data points and the modified Poisson curves in Fig. 5.

Figure 6 shows the dependence of $\langle n\rangle$ on the center-of-mass energy for this experiment and for other e^+e^- experiments, including recent results at $\sqrt{s}=91$ GeV.[10,11,26,27] The variation of $\langle n\rangle$ with $\sqrt{s}$, for all of the data shown in Fig. 6, was fitted with the following functions.

(1) Fitting to the form derived from the fireball and hydrodynamical models for hadron-hadron interactions,[28]

$$\langle n\rangle = as^b ,$$

yields $a=2.20\pm0.03$ and $b=0.252\pm0.002$ with $\chi^2=143$ for 86 degrees of freedom ($N_{\rm DF}$). Note that the fitted value for the exponent b is consistent with the $s^{1/4}$ behavior first predicted by Fermi.[2] The results of this fit are shown in Fig. 6 as a solid curve.

(2) Fitting to the empirical relationship from analyses of pp data,[6]

TABLE III. Summaries of the multiplicity distributions at each energy. The entries are the number of selected events; the integrated luminosity L; the average multiplicity $\langle n\rangle$; the rms dispersion D; the f_2 moment where $f_2=D^2-\langle n\rangle$; the average multiplicity divided by the dispersion; and the results of fitting the KNO plot to a Γ distribution (fit parameter $=K$) and a negative-binomial distribution (fit parameter$=k$). The results for all the data combined ($\langle\sqrt{s}\rangle=57$ GeV) are given in the last column, where the second error listed indicates our estimate of the systematic error.

$\sqrt{s}$	50 GeV	52 GeV	55 GeV	56 GeV	57 GeV
No. events	77	396	288	604	393
L (pb^{-1})	0.64±0.02	3.98±0.04	3.27±0.04	5.99±0.05	4.40±0.05
$\langle n\rangle$	16.24±0.41	16.74±0.19	16.82±0.22	17.27±0.16	17.49±0.19
D	4.78±0.28	5.00±0.17	4.95±0.17	5.20±0.13	5.19±0.17
f_2	6.66±2.71	8.32±1.66	7.66±1.73	9.80±1.37	9.54±1.73
$\langle n\rangle/D$	3.40±0.22	3.35±0.12	3.40±0.13	3.32±0.08	3.37±0.11
K GD fit	11.9±0.8	11.7±0.6	11.6±0.8	13.3±0.4	11.1±0.7
$\chi^2/N_{\rm DF}$	5/18	8/18	6/18	23/18	7/18
k NB fit	71.0±2.5	47.7±7.4	56.5±8.8	46.7±5.6	46.2±6.2
$\chi^2/N_{\rm DF}$	6/18	8/18	5/18	9/18	8/18

$\sqrt{s}$	60 GeV	60.8 GeV	61.4 GeV	$\langle\sqrt{s}\rangle=57$ GeV (Combined)
No. events	320	299	363	2740
L (pb^{-1})	3.55±0.04	3.49±0.05	4.33±0.05	29.6
$\langle n\rangle$	17.85±0.23	17.66±0.23	17.61±0.21	17.19±0.07±0.48
D	5.43±0.21	5.29±0.18	5.35±0.17	5.03±0.06±0.25
f_2	11.63±2.26	10.41±1.93	11.09±1.87	8.11±0.59
$\langle n\rangle/D$	3.29±0.13	3.34±0.12	3.29±0.11	3.42±0.04
K GD fit	13.2±0.4	14.8±0.3	13.1±0.4	12.0±0.4
$\chi^2/N_{\rm DF}$	19/19	32/19	23/19	18/19
k NB fit	40.1±4.7	63.8±8.9	55.4±7.4	52.8±4.3
$\chi^2/N_{\rm DF}$	7/19	16/19	18/19	21/19

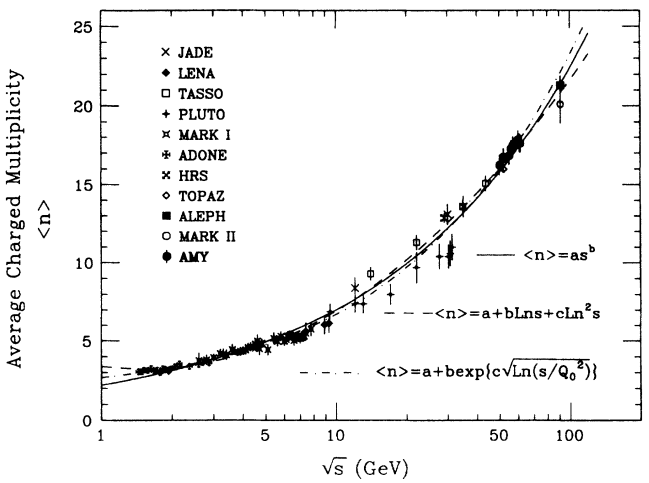

FIG. 6. The average charged multiplicity in e^+e^- annihilation as a function of center-of-mass energy $\sqrt{s}$, including results from other experiments. The errors shown are the quadrature sum of the statistical and systematic errors. The curves show the fits to the data (see text).

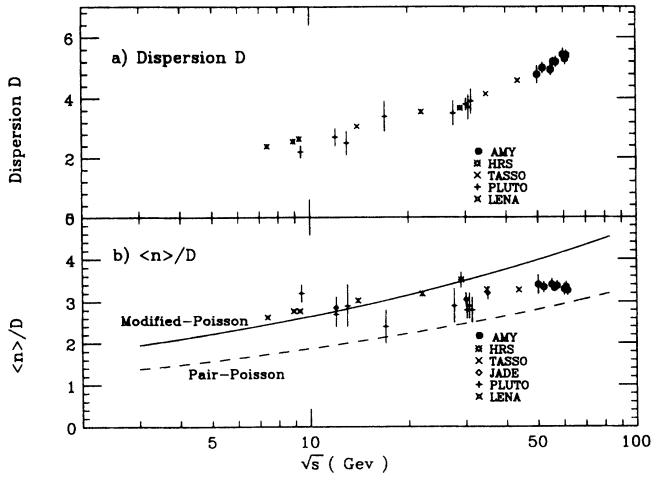

FIG. 7. (a) The energy dependence of the dispersion D. (b) The energy dependence of $\langle n \rangle / D$. The dashed curve is the expectation for a pair Poisson behavior; the solid curve is that for a modified Poisson. Only the statistical errors are shown.

$$\langle n \rangle = a + b \ln s + c \ln^2 s \ ,$$

yields $a = 3.37 \pm 0.09$, $b = -0.43 \pm 0.06$, and $c = 0.262 \pm 0.007$ with $\chi^2 = 93$ for 85 $N_{\rm DF}$. This fit is shown as a dashed curve in Fig. 6.

(3) Fitting to the form suggested by leading-logarithm QCD,[3–5]

$$\langle n \rangle = a + b \exp\{c[\ln(s/Q_0^2)]^{1/2}\} \ ,$$

with Q_0 taken to be 1 GeV, gives $a = 2.59 \pm 0.08$, $b = 0.085 \pm 0.010$, and $c = 1.81 \pm 0.04$, with $\chi^2 = 85$ for 85 $N_{\rm DF}$. The fit is shown as a dotted-dashed curve in Fig. 6.

In fact, the above curves are not expected to be precise representations of the charged multiplicity at lower energies where resonances and thresholds are expected to produce small-scale fluctuations. If we limit the fits to center-of-mass energies above 5 GeV, well above the threshold for charmed-particle production, the three cases give fits of similar quality ($\chi^2/N_{\rm DF} = 69/50$, 60/49, and 61/49 for cases 1, 2, and 3, respectively). All of the above functions describe the high-energy data equally well; differences between them only become significant at center-of-mass energies above 100 GeV.

Figure 7(a) shows the dispersion D as a function of $\sqrt{s}$. The error bars shown are statistical only; the systematic uncertainties are about 5.0% of the D values. The D values measured in lower-energy experiments are also shown in the figure.

The ratio $\langle n \rangle / D$ is shown as a function of energy in Fig. 7(b), both for this experiment and for previous experiments. This shows some weak energy dependence, increasing slightly with increasing $\sqrt{s}$. The solid (dashed) curve in Fig. 7(b) shows the expectations for a modified Poisson (pair Poisson) behavior of the multiplicity distribution; both cases clearly differ from the measured points.

In Fig. 8 we present the KNO distribution for all of our data combined ($\langle \sqrt{s} \rangle = 57$ GeV) together with the 29-GeV data from the HRS experiment,[10] and the 34.8-GeV data from the TASSO experiment.[11] There is no marked change in the KNO distribution over the center-of-mass range from 29 to 57 GeV. Fitting the data from the three experiments to a Γ distribution (GD) [Eq. (1)] gives values of K of

$$K = 12.0 \pm 0.4 \quad (\chi^2/N_{\rm DF} = 18/19) \quad \text{AMY (57 GeV)} \ ,$$

$$K = 10.9 \pm 0.1 \quad (\chi^2/N_{\rm DF} = 71/17) \quad \text{TASSO (34.8 GeV)} \ ,$$

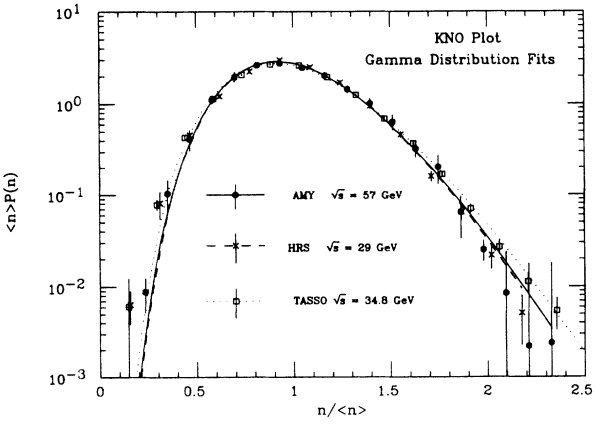

FIG. 8. The KNO charged multiplicity distribution for the combined data of this experiment compared with measurements at lower energies and with the fitted Γ distributions. The vertical axis is the normalized charged multiplicity distribution scaled by the average multiplicity $\langle n \rangle$; the horizontal axis is the scaled multiplicity $n/\langle n \rangle$. For the HRS and AMY results, the errors shown are the quadrature sum of the statistical and systematic errors; only statistical errors are shown for the TASSO data.

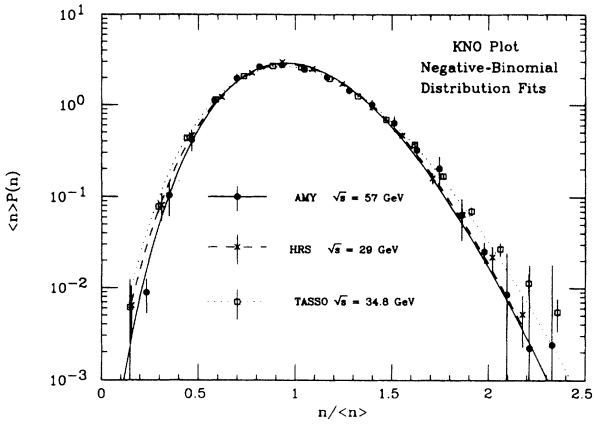

FIG. 9. The KNO charged multiplicity distribution for the combined data of this experiment compared with measurements at lower energies and with the fitted negative-binomial distributions. Here the errors are the same as in Fig. 8.

$K=12.3\pm0.3$ $(\chi^2/N_{\rm DF}=41/13)$ HRS (29.0 GeV).

While the GD shape provides poor fits for the HRS and TASSO data, it fits our data reasonably well. We have fitted the same data to a negative-binomial (NB) distribution [Eq. (2)]. The results of these fits are

$k=52.8\pm4.3$ $(\chi^2/N_{\rm DF}=21/19)$ AMY(57 GeV),

$k=54.1\pm3.1$ $(\chi^2/N_{\rm DF}=39/17)$ TASSO (34.8 GeV),

$k=233.5.0\pm53.2$ $(\chi^2/N_{\rm DF}=7/13)$ HRS (29.0 GeV),

and are shown as solid, dotted, and dashed curves in Fig. 9, respectively. Note that the NB distribution depends both on k and $\langle n\rangle$, so although the values of k derived from our data and from the HRS results differ, the actual curves agree quite well, leading us to conclude that KNO scaling works well over this energy range. Results for GD and NB fits to the distributions at each of the eight center-of-mass energies and for all the energies combined are given in Table III.

VIII. DISCUSSION

We have presented the multiplicity distributions for charged particles produced in e^+e^- annihilation at center-of-mass energies ranging from 50 to 61.4 GeV. The charged-particle multiplicity distributions are well reproduced by the LUND 6.3 parton-shower model.

The average charged-particle multiplicity $\langle n\rangle$ is found to rise with center-of-mass energy and is fitted equally well by Fermi's prediction $\langle n\rangle=as^{1/4}$, the empirical relation $\langle n\rangle=a+b\ln s+c\ln^2 s$, and the QCD-motivated form $\langle n\rangle=a+b\exp\{c[\ln(s/Q_0^2)]^{1/2}\}$. The multiplicity distributions are found to deviate significantly from the modified Poisson distribution at TRISTAN energies. While experiments at lower energy ($\sqrt{s}=29$ GeV) show good agreement with a modified Poisson distribution,[10] our results confirm the trend toward distributions that are wider than Poisson-like distributions that was first observed at $\sqrt{s}\geq34.8$ GeV.[11] The distributions follow KNO scaling; both the Γ and the negative-binomial distribution functions fit our measured KNO distributions well.

ACKNOWLEDGMENTS

We thank the TRISTAN staff for the excellent operation of the storage ring. In addition we acknowledge the strong support and enthusiastic assistance provided by the staffs of our home institutions. We thank W. Bartel for many helpful comments. This work has been supported by the Japan Ministry of Education, Science and Culture (Monbusho), the U.S. Department of Energy and National Science Foundation, The Korea Science and Engineering Foundation and Ministry of Education, and the Academia Sinica of the People's Republic of China.

[1]W. Heisenberg, Z. Phys. **113**, 61 (1939); Nature (London) **164**, 65 (1949).
[2]E. Fermi, Prog. Theor. Phys. **5**, 570 (1950).
[3]W. Furmanski, R. Petronzio, and S. Pokoski, Nucl. Phys. **B155**, 253 (1979).
[4]A. Bassetto, M. Ciafaloni, and G. Marchesini, Phys. Lett. **83B**, 207 (1978).
[5]A. Mueller, Phys. Lett. **104B**, 161 (1981); Nucl. Phys. **B213**, 85 (1983).
[6]W. Thome *et al.*, Nucl. Phys. **B129**, 365 (1977).
[7]Z. Koba, H. B. Nielsen, and P. Olesen, Nucl. Phys. **B40**, 317 (1972).
[8]R. P. Feynman, Phys. Rev. Lett. **23**, 1415 (1969).
[9]T. T. Chou and C. N. Yang, Int. J. Mod. Phys. A **2**, 1727 (1987); Phys. Lett. **167B**, 453 (1986).
[10]HRS Collaboration, M. Derrick *et al.*, Phys. Rev. D **34**, 3304 (1986); Z. Phys. C **35**, 323 (1987).
[11]TASSO Collaboration, M. Althoff *et al.*, Z. Phys. C **22**, 307 (1984); W. Braunschweig *et al.*, *ibid.* **45**, 193 (1989).
[12]A. Giovannini and L. Van Hove, Acta Phys. Pol. B **19**, 495 (1988), and references cited therein; Z. Phys. C **30**, 391 (1986).
[13]P. Carruthers and C. Shih, Int. J. Mod. Phys. A **2**, 1447 (1987), and references cited therein.
[14]C. K. Chew and Y. K. Lim, Phys. Lett. **163B**, 257 (1985).
[15]UA5 Collaboration, R. E. Ansorge *et al.*, Z. Phys. C **43**, 357 (1989).
[16]T. Sjostrand and M. Bengtsson, Comput. Phys. Commun. **43**, 367 (1987).
[17]AMY Collaboration, T. Kumita *et al.*, Phys. Rev. D (to be published). See also AMY Collaboration, H. Sagawa *et al.*, Phys. Rev. Lett. **60**, 93 (1988).
[18]T. Mori, Ph.D. thesis, University of Rochester, 1988.
[19]The parameters used in the LUND 6.3 (parton-shower) model are $\Lambda_{\rm LLA}=0.40$ GeV; cascade virtuality cutoff $Q_0=1.0$ GeV; fragmentation parameter $a=0.50$; fragmentation parameter $b=0.9$ GeV^{-2}; Gaussian P_T parameter $\sigma_q=0.35$ GeV/c.
[20]H. W. Zheng, Ph.D. thesis, University of Rochester, 1990.
[21]All charged particles from $K_S^0\to\pi^+\pi^-$ ($c\tau=2.675$ cm) and

$\Lambda^0 \to p\pi^-$ ($c\tau = 7.89$ cm) are included in the corrected charged multiplicity, even though there is some chance for the decays to occur far from the vertex. In the LUND 6.3 model, the average number of charged particles per event from $K_S^0 \to \pi^+\pi^-$ and $\Lambda^0 \to p\pi^-$ (plus $\bar{\Lambda}^0 \to \bar{p}\pi^+$) are 1.14 and 0.28, respectively.

[22]A. Grant, Nucl. Instrum. Methods **131**, 167 (1975).

[23]AMY Collaboration, Y. K. Li *et al.*, Phys. Rev. D **41**, 2675 (1990).

[24]T. Sjostrand, Comput. Phys. Commun. **39**, 347 (1986).

[25]If we compare the observed charged multiplicity distribution with that expected from the LUND 6.3 (parton-shower) model [Fig. 2(a)], we find a $\chi^2/N_{\rm DF} = 1.3$. A similar comparison for the LUND 6.2 (matrix element) model [Fig. 2(b)] yields a $\chi^2/N_{\rm DF} = 3.6$. We use a mixture of equal numbers of events for LUND 6.2 and 6.3 ($\chi^2/N_{\rm DF} = 2.0$) as a reasonably extreme variation of the MC generator for purposes of estimating the associated systematic error.

[26]ADONE Collaboration, C. Bacci *et al.*, Phys. Lett. **86B**, 234 (1979); PLUTO Collaboration, C. Berger *et al.*, *ibid.* **95B**, 313 (1980); LENA Collaboration, B. Niczyporuk *et al.*, Z. Phys. C **9**, 1 (1981); Mark I Collaboration, J. L. Siegrist *et al.*, Phys. Rev. D **26**, 969 (1982); JADE Collaboration, W. Bartel *et al.*, Z. Phys. C **20**, 187 (1983); TOPAZ Collaboration, M. Yamauchi, in *Proceedings of the XXIV International Conference on High Energy Physics*, Munich, West Germany, 1988, edited by R. Kotthaus and J. H. Kuhn (Springer, Berlin, 1988).

[27]ALEPH Collaboration, D. Decamp *et al.*, Phys. Lett. B **234**, 209 (1990); Mark II Collaboration, G. S. Abrams *et al.*, Phys. Rev. Lett. **64**, 1334 (1990).

[28]H. Satz, in *Current Induced Reactions*, edited by J. G. Körner, G. Kramer, and D. Schildknecht (Lecture Notes in Physics, Vol. 56) (Springer-Verlag, Berlin, 1975), p. 49.